Thermodynamics of the Formation of $MgO-Al_2O_3-TiO_x$ Inclusions in Ti-Stabilized 11Cr Ferritic Stainless Steel

JOO HYUN PARK, SANG-BEOM LEE, and HENRI R. GAYE

The equilibration between $CaO-SiO_2-MgO-Al_2O_3-CaF_2$ ($-TiO_2$) slag and Fe-11 mass pct Cr ferritic stainless steel melts was investigated at 1873 K in order to clarify the effect of Al and Ti addition as well as that of slag composition on the formation of complex oxide inclusions. The activity of oxygen calculated from the classical Wagner formalism changes from about $a_O = 0.0002$ to 0.001 and the values of a_O from [Al]/(Al_2O_3) and that from [Si]/(SiO_2) equilibria are in relatively good agreement with each other with some scatters. The phase stability diagram of the inclusions and the equilibrium iso-[O] lines in the Fe-11 mass pct Cr-0.5 mass pct Si-0.3 mass pct Mn-0.0005 mass pct Mg steel melts was constructed by using FACTSAGE 5.5 program as a function of Al and Ti contents. The computed iso-[O] lines were slightly larger than the values estimated from the slag-metal equilibria. The composition of the inclusions could be plotted on the computed $MgO-Al_2O_3-TiO_x$ phase diagram. The inclusions in the steel melts equilibrated with the basic slags are located in the "spinel + liquid" region, while those in equilibrium with the less basic slags are mostly in the "liquid" single phase. This is in good accordance to the observed morphology of the inclusions. However, in cases of high concentration of Ti and Al, the inclusions were found to be spinel + liquid, even though the less basic slags are equilibrated. When plotted on logarithmic scales, the mole ratio $\left(X_{MgO} \times X_{Al_2O_3}/X_{Ti_2O_3}\right)$ of the inclusions (spinel potential) was expressed as a linear function of $\left[a_{Mg} \times a_{Al}^2 \times a_O/a_{Ti}^2\right]$ of the steel melts with a slope of unity theoretically expected. Also, the spinel potential is very low and nearly constant when the activity of Al_2O_3 is less than that of TiO_2 in the slag saturated by MgO, whereas it linearly increases by increasing the log $(a_{Al_2O_3}/a_{TiO_2})$ at $(X_{Al_2O_3}/X_{TiO_2}) > 1$.

DOI: 10.1007/s11663-008-9172-4

I. INTRODUCTION

TITANIUM-STABILIZED ferritic stainless steels have been the subject of previous studies related to clogging of the submerged entry nozzle (SEN) during continuous casting process and control of the solidification structure through heterogeneous nucleation by the inclusions containing titanium oxide or nitride. In view of productivity of the melt shops and surface quality (sliver, flaw, or crack) of steel products, it is desirable to have the amount of inclusions as low as possible.[1–7] On the contrary, the use of inclusions is expected to help produce fine grains during primary solidification, which is preferable to other methodologies such as controlled deformation and heat treatment.[8,9] In these studies, the $MgAl_2O_4$ spinel inclusion could accelerate the formation of TiN in molten steel due to very low disregistry between them, and finally an equiaxed fine-grained structure was produced by the heterogeneous nucleation of delta ferrites on the TiN particles.

Clogging phenomena of SEN or tundish nozzle during continuous casting of Ti-stabilized stainless steels have been investigated by several researchers. Hasegawa *et al.*[1] observed that the constriction of tundish nozzle becomes more severe as the ratio of Al_2O_3 to TiN increases and that the main origin of these particles is the reaction between aluminum in the stainless steel melt (type 321) and silica in the refractory, as well as the reaction products in deoxidation and nitrogen removal processes. They assumed that the buildup originated not only from the deposition of nonmetallic inclusions, but also from freezing of the steel. Gao and Sorimachi proposed that the globular Ti oxide could be formed by the reoxidation of TiN in type 409 stainless steel.[2] Their findings indicated that the major materials deposited in an immersed nozzle were globular Ti oxide and alumina agglomerates, whereas TiN and Al_2O_3 were observed in molten steel in the tundish along with a minor amount of Ti oxides. Maddalena *et al.*[3] reported that the presence of magnesium aluminate spinel in the stainless steels (types 321 and 409) accelerates the growth of the deposits from their observation of two distinct types of TiN-based deposits during analysis of clogged nozzles; pure TiN in

JOO HYUN PARK and SANG-BEOM LEE, Senior Researchers, are with the Stainless Steel Research Group, Technical Research Laboratories, POSCO, Pohang 790-785, Korea. Contact e-mail: basicity@yahoo.co.kr HENRI R. GAYE, Professor, is with the Clean Steel Laboratory, Graduate Institute of Ferrous Technology (GIFT), POSTECH, Pohang 790-784, Korea.

Manuscript submitted January 20, 2008.
Article published online November 11, 2008.

a three-dimensional array and TiN particles apparently connected *via* spinel phase. Recently, Nunnington and Sutcliffe reported that the main solubility product inclusions include Al_2O_3, Ti_3O_5, TiN, $MgAl_2O_4$, and Al_2TiO_5, and sometimes the precipitation of $CaTiO_3$ (perovskite) in slag-type inclusions could be found in the stainless steels (types 321 and 409).[4] In addition, they observed the oxidation of TiN inclusion in type 441 stainless steel and postulated the formation of titanium oxynitride, $Ti(ON)_{ss}$ from the high mutual solid solubility of TiO and TiN in the cubic structure.[10] Zheng *et al*.[5] also experienced two types of SEN clogging, *viz*. TiN and $CaTiO_3$ in the stainless steel (type 321). The former was associated with the TiN containing $MgAl_2O_4$ core as well as the simple TiN inclusion, and the latter consisted of $CaTiO_3$-$MgAl_2O_4$ dual phase inclusion. The effect of aluminum and titanium deoxidation on the formation of $CaTiO_3$-$MgAl_2O_4$ dual phase inclusion was formerly investigated by Kim *et al*.[6,7] for type 304 and 430 stainless steels. Even though these studies described well the phenomena of the clogging and inclusions in the stainless steel industry, thermodynamic understanding for the effect of slag composition on the complex oxides in Ti-stabilized ferritic stainless steel is still insufficient.

Liao and Fruehan investigated the formation condition of Al_2O_3, AlN, Ti_3O_5, and TiN inclusions by deoxidation of type 304 stainless steel from the effect of chromium on the activity coefficient of titanium and aluminum.[11] Jo *et al*.[12] reported that the titanium deoxidation would not be recommended in view of the formation of $MgAl_2O_4$ inclusion in the Fe-18 mass pct Cr stainless steel because the dissolution of magnesium from slag or refractory could be enhanced due to the high affinity between titanium and magnesium. However, they did not focus on the effect of slag composition on the formation of inclusions in the stainless steel melts.

In-depth thermodynamic and kinetic studies on the effect of slag on the formation mechanism of spinel inclusions in Ti-free 16 mass pct Cr ferritic stainless steel have been investigated by Park and Kim[13] and Okuyama *et al*.,[14] respectively. In the former study, the composition of the inclusion was strongly affected by that of top slag. For example, the more basic slag (CaO or MgO saturation) equilibrated with the molten steel, the more MgO-rich spinel inclusions were observed.[13] In the latter, the slag/metal and metal/inclusion reaction kinetics were investigated in aluminum deoxidation condition. The concentration of MgO in the inclusions increased by increasing the ratio of CaO to SiO_2 (or Al_2O_3) in the top slag and the rate determining step was proposed as a diffusion of magnesium in molten steel.[14] Therefore, in the present study, based on the preceding view of thermodynamic and kinetic studies, the equilibration between CaO-SiO_2-MgO-Al_2O_3-CaF_2 (-TiO_2) slag and Ti-stabilized Fe-11 mass pct Cr ferritic stainless steel melts has been investigated at 1873 K in order to clarify the effect of aluminum and titanium addition, as well as that of slag composition, on the formation of complex oxide inclusions containing titanium.

II. EXPERIMENTAL

Pure iron, chromium, silicon, and manganese (>99.9 mass pct reagent grade Fe, Cr, Si, and Mn) were premelted in a vacuum induction furnace to make a nominal composition of Fe-11 mass pct Cr-0.5 mass pct Si-0.3 mass pct Mn ferritic stainless steel. Alloys of about 730 g and the premelted CaO-SiO_2-MgO-Al_2O_3-4 mass pct CaF_2 slags (B = (mass pct CaO + mass pct MgO)/(mass pct SiO_2 + mass pct Al_2O_3) = 0.9 to 1.7)) of about 20 to 30 g were equilibrated in pure MgO (>99.9 mass pct, MgO-S(3N), TEP Corp., Tokyo) crucibles at 1873 K, heated in a high-frequency induction furnace. The initial contents of dissolved aluminum and titanium in the premelted alloy were approximately less than 25 ppm.

The stainless steel reaction chamber, which was cooled by cooling water, was initially evacuated by the mechanical rotary pump and filled by Ar gas (1.01×10^5 Pa) and followed by induction heating. The temperature was established to be 1873 K using an *R*-type (Pt-13 mass pct Rh/Pt) thermocouple and a proportional integral differential controller. Any possible interference of high frequency on temperature detecting was reduced by grounding the circuit of thermocouple. Preliminary trials confirmed that the radio frequency interference was not significant in the present experimental setup and the temperature fluctuation of steel melts could be controlled within ±3 K during experiments. The oxygen in Ar gas was removed by passing the gas through magnesium turnings heated to about 773 K, even though 99.999 pct purity Ar gas was used. After the steel samples were melted at 1873 K, the premelted slags were added and followed by the addition of aluminum less than about 200 ppm. After 3 minutes, a fixed amount of sponge titanium equivalent to about 0.3 mass pct was added. All of the additives, such as slags and metals, were dropped through the quartz tube under an inert atmosphere. Then the system was equilibrated during about 60 minutes, which was determined by the preliminary equilibrium experiments. That is, the concentration of MgO, SiO_2, Al_2O_3, and TiO_2 in the slag, as well as titanium and aluminum in the steel melt, showed a constant value approximately within 40 minutes. Thus, it was confirmed that the slag was saturated by MgO. After equilibrating, the power of the furnace was turned off and the crucible assembly was quenched by helium gas, which was blown from the top surface of the crucible. A schematic diagram of the experimental apparatus is shown in Figure 1.[15–17]

The metal and slag samples were prepared for chemical analysis. The content of major components such as chromium, silicon, manganese, and total aluminum were analyzed by optical emission spectrometry and the content of dissolved aluminum, titanium, and magnesium was determined by the inductively-coupled plasma spectroscope (ICP-AES, IRIS Advantage (REG), Thermo Electron, Waltham, MA). The content of oxygen and nitrogen was analyzed by fusion and the infrared absorption method after very careful preparation through an ultrasonic cleaning. The composition of the slag was analyzed by an X-ray fluorescence

spectroscope (SRS3400, Bruker AXS, Cheshire, United Kingdom). The final compositions of steel and slag are listed in Tables I and II. Here, the presence of titanium oxide in the slag did not originate from initial addition but from slag/metal reactions that occur to achieve equilibrium.

The metal samples were mounted in cold-setting resin. Next, standard grinding and polishing techniques were used, after which all samples were gold coated. Finally, the compositions of about ten inclusions per sample were determined by using a scanning electron microscope and energy dispersive spectroscope (SEM-EDS, JSM-840A, JEOL*) with a link detector.

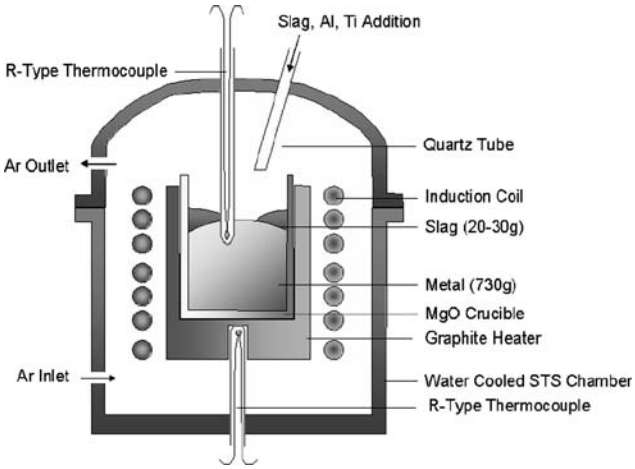

Fig. 1—Schematic diagram of the experimental apparatus.

*JEOL is a trademark of Japan Electron Optics Ltd., Tokyo.

The composition of the inclusion in each sample was taken from the average value of about ten inclusions. In some experimental samples, the oxide-TiN complex inclusions were found in the middle part of the sample. From the thermodynamic calculation based on the steel compositions listed in Table II, the TiN could be formed at about 1723 (±20) K. This indicates that the TiN inclusions were formed during cooling of steel samples, even though we tried to quench the samples. Thus, in this case, the oxide inclusions that are not incorporated to TiN in the upper part of the steel samples were selected and analyzed by EDS.

III. RESULTS AND DISCUSSION

A. *Thermodynamics of Deoxidation and Inclusion Composition in Fe-11Cr Stainless Steel Equilibrated with CaO-SiO_2-MgO-Al_2O_3-CaF_2 (-TiO_2) Slags*

The addition of aluminum into the silicon deoxidized Fe-11 mass pct Cr-0.5 mass pct Si-0.3 mass pct Mn stainless steel changes the activity of oxygen in the melt,

Table I. Equilibrium Composition of Slags in the Present Study (Mass Percent)

Run	CaO	Al_2O_3	SiO_2	TiO_2	CaF_2	MgO
10M-0	42.6	6.1	19.5	14.7	6.7	10.4
10M-1	42.8	12.8	16.2	12.5	5.5	10.3
10M-2	44.2	15.7	14.8	11.4	4.2	9.7
10M-7	42.0	16.0	11.5	14.4	6.3	9.8
10M-8	43.0	18.7	9.0	13.1	6.9	9.3
18M-3	33.9	5.2	25.8	12.8	6.1	16.2
18M-4	31.5	7.6	26.1	12.1	4.1	18.5
18M-5	31.7	9.5	26.4	10.9	3.2	18.4
18M-6	31.3	12.1	25.5	9.8	3.8	17.4
18M-9	32.3	14.2	20.0	12.5	5.4	15.7
18M-10	31.4	16.1	19.0	12.2	5.1	16.2
18M-5A	30.9	9.7	31.8	4.5	3.6	19.5

Table II. Equilibrium Composition of Steel Melts in the Present Study (Mass Percent)

Run	Cr	Si	Mn	Total O	Dissolved O	Total Al	Dissolved Al	Ti	Mg	N
10M-0	11.1	0.47	0.29	0.0023	0.00200	0.0035	0.0007	0.036	0.0007	0.014
10M-1	11.2	0.46	0.28	0.0029	0.00151	0.0035	0.0015	0.023	0.0004	0.008
10M-2	11.1	0.44	0.29	0.0018	0.00134	0.0045	0.0021	0.035	0.0004	0.010
10M-7	11.0	0.59	0.28	0.0032	0.00068	0.0074	0.0068	0.071	0.0003	0.016
10M-8	11.0	0.59	0.29	0.0023	0.00057	0.0113	0.0110	0.100	0.0003	0.021
18M-3	11.1	0.49	0.29	0.0023	0.00169	0.0020	0.0003	0.020	0.0003	0.010
18M-4	11.1	0.49	0.28	0.0024	0.00216	0.0020	0.0003	0.013	0.0004	0.012
18M-5	11.1	0.51	0.29	0.0024	0.00188	0.0021	0.0004	0.015	0.0004	0.013
18M-6	11.0	0.46	0.28	0.0030	0.00183	0.0020	0.0004	0.010	0.0004	0.013
18M-9	11.0	0.60	0.29	0.0024	0.00157	0.0045	0.0028	0.029	0.0003	0.014
18M-10	11.0	0.62	0.28	0.0025	0.00167	0.0043	0.0022	0.024	0.0003	0.015
18M-5A	11.1	0.40	0.28	0.0034	0.00251	0.0017	0.0004	0.005	0.0004	0.016

which is also affected by the equilibrium between metal phase and slag phase. The equilibrium deoxidation reaction by aluminum and silicon is given in Eqs. [1] and [3], respectively.[18,19]

$$2[\mathrm{Al}] + 3[\mathrm{O}] = (\mathrm{Al_2O_3})^{\mathrm{slag}} \quad [1]$$

$$\log\ K_{[1]} = \log\ \left[\frac{a_{\mathrm{Al_2O_3}}}{a_{\mathrm{Al}}^2 \times a_{\mathrm{O}}^3}\right] = \frac{45{,}300}{T} - 11.62 \quad [2]$$

$$[\mathrm{Si}] + 2[\mathrm{O}] = (\mathrm{SiO_2})^{\mathrm{slag}} \quad [3]$$

$$\log\ K_{[3]} = \log\ \left[\frac{a_{\mathrm{SiO_2}}}{a_{\mathrm{Si}} \times a_{\mathrm{O}}^2}\right] = \frac{24{,}600}{T} - 8.4 \quad [4]$$

where $K_{[n]}$ and a_i are the equilibrium constant of Eq. [n] and the activity of element i in the steel melt. The activity of oxygen determined by the equilibrium of $[\mathrm{Al}]/(\mathrm{Al_2O_3})$, $a_{\mathrm{O}}^{\mathrm{Al}}$ and by $[\mathrm{Si}]/(\mathrm{SiO_2})$, $a_{\mathrm{O}}^{\mathrm{Si}}$ can be estimated from Eqs. [5] and [6], respectively.

$$\log\ a_{\mathrm{O}}^{\mathrm{Al}} = \frac{1}{3}\ (\log\ a_{\mathrm{Al_2O_3}} - 2\log\ a_{\mathrm{Al}} - \log\ K_{[1]}) \quad [5]$$

$$\log\ a_{\mathrm{O}}^{\mathrm{Si}} = \frac{1}{2}\ (\log\ a_{\mathrm{SiO_2}} - \log\ a_{\mathrm{Si}} - \log\ K_{[3]}) \quad [6]$$

In addition, the activity coefficient of solute element (M) can also be calculated by the classical Wagner formalism using the first- and second-order interaction parameters, which are listed in Table III.[12,18,20–29]

$$\log\ f_{\mathrm{M}} = \sum_{\mathrm{i=Cr,Si,Mn,Al,Ti,Mg,O}} \left(e_{\mathrm{M}}^{\mathrm{i}} \times [\text{mass pct i}] + r_{\mathrm{M}}^{\mathrm{i}} \times [\text{mass pct i}]^2\right) \quad [7]$$

where f_{M}, e, and r are, respectively, the Henrian activity coefficient of element M, and the first- and second-order interaction parameters between each element. In Figure 2, the activities of oxygen calculated from the $[\mathrm{Al}]/(\mathrm{Al_2O_3})$ equilibrium and that from the $[\mathrm{Si}]/(\mathrm{SiO_2})$ equilibrium are plotted against the activity of oxygen from the classical Wagner formalism, where the concentration of dissolved oxygen was taken by the average of oxygen determined from $[\mathrm{Al}]/(\mathrm{Al_2O_3})$ and $[\mathrm{Si}]/(\mathrm{SiO_2})$ equilibria, and is listed in Table II. Also, the activity of $\mathrm{Al_2O_3}$ and $\mathrm{SiO_2}$ in the slag at 1873 K was taken from the

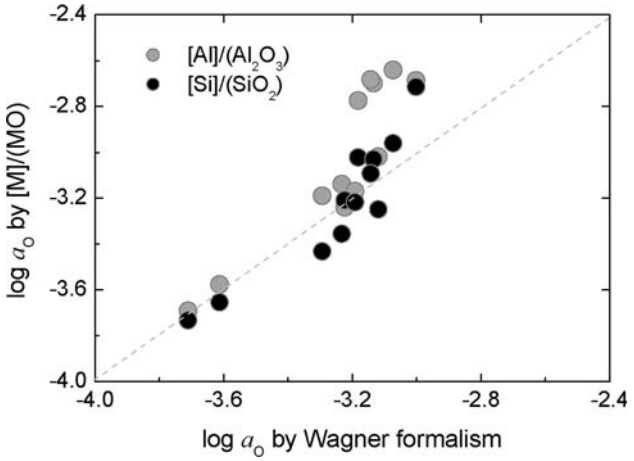

Fig. 2—Relationship between activities of oxygen calculated from classical Wagner formalism and deoxidation equilibria by aluminum and silicon in Fe-11 mass pct Cr-0.5 mass pct Si-0.3 mass pct Mn-Al-Ti melt equilibrated with $\mathrm{CaO\text{-}SiO_2\text{-}MgO\text{-}Al_2O_3\text{-}CaF_2\text{-}TiO_2}$ slag at 1873 K.

thermodynamic data reported by Ohta and Suito by assuming that the effect of about 5 mass pct $\mathrm{CaF_2}$ and 12 mass pct $\mathrm{TiO_2}$ would not seriously affect the activity coefficient of $\mathrm{SiO_2}$ and $\mathrm{Al_2O_3}$.[30] The activity of oxygen from the classical Wagner formalism changes from about $\log a_{\mathrm{O}} = -3.7$ to -2.9, and the values of $a_{\mathrm{O}}^{\mathrm{Al}}$ and $a_{\mathrm{O}}^{\mathrm{Si}}$ are in relatively good correspondence to each other with some scatters. This tendency shows fair accordance to the thermodynamic equilibrium of the present slag-metal system, which has been discussed by one of the authors (HRG) and co-workers.[31,32] on the basis of thermodynamic model (IRSID slag model) and experimental data.

The equilibrium oxygen content and the stability diagram of the inclusions in the Fe-11 mass pct Cr-0.5 mass pct Si-0.3 mass pct Mn-0.014 mass pct N steel melt containing 5 mass ppm Mg, and Al and Ti, was calculated with the aid of thermodynamic software, FACTSAGE (version 5.5)** using "FACT53" (FACT 5.3 compound), "FToxid" (FACT oxide), and "FSstel" (FACTSAGE steel alloy) databases.[33]

The specific description and details regarding the associate model and parameters are found in the recent

**FactSage is a trademark of ESM software, Hamilton, OH.

Table III. Interaction Parameters used in the Present Study

e_{ij} (r_{ij})	Cr	Si	Mn	Al	Ti	Mg	O
Al	0.030[21]	0.056	0.035[22]	0.043	0.016[23]	−0.30[12]	−1.98[18] (39.82)
Ti	0.029[24]	−0.025[25]	−0.043	0.024[23]	0.042	−1.27[12]*	−1.62[26] (−0.36)
Si	−0.021[19]	0.10	−0.007*	0.058	−0.013*	−0.11*	−0.12
Mg	0.022[12]	−0.096[12]	—	−0.27[12]	−0.64[12]	—	560[27] (145,000)
O	−0.032[28]	−0.066	−0.037[29]	−1.17[18] (−0.010)	−0.54[26] (0.039)	−370[27] (5,900)	−0.17

*Calculated from the relation $e_j^{(i)} = \frac{M_i}{M_j} e_i^{(j)} + 0.434 \times 10^{-2} \frac{M_i - M_j}{M_j}$.[45]

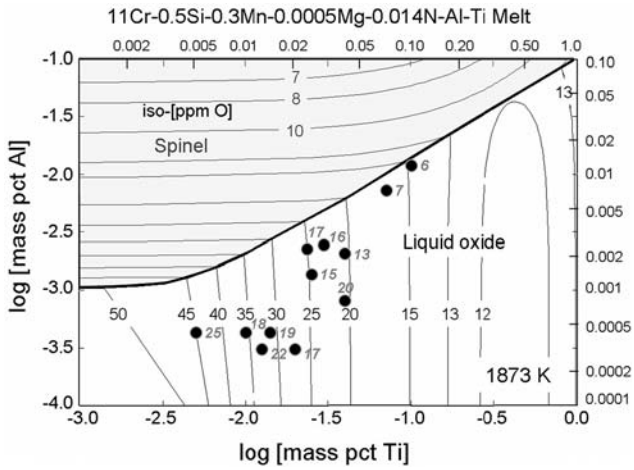

Fig. 3—Computed stability diagram of inclusions and iso-[O] lines in the Fe-11 mass pct Cr-0.5 mass pct Si-0.3 mass pct Mn-0.0005 mass pct Mg-Al-Ti melt equilibrated the $CaO\text{-}SiO_2\text{-}MgO\text{-}Al_2O_3\text{-}CaF_2\text{-}TiO_2$ slag at 1873 K. Solid circles are experimental points with dissolved oxygen content.

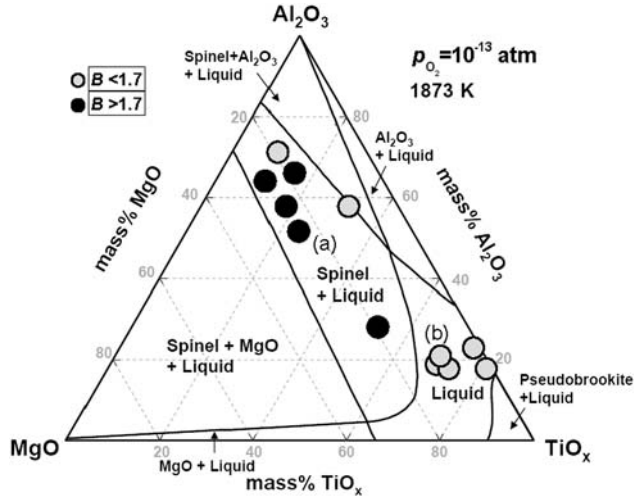

Fig. 4—Computed phase diagram of $MgO\text{-}Al_2O_3\text{-}TiO_x$ system at 1873 K and $p_{O_2} = 10^{-13}$atm. Circles are the average composition of ten inclusions per sample.

study by Jung *et al.*[34] Figure 3 shows the computed stability diagram of the inclusions at 1873 K in the composition range of [Ti] = 0.001 to 1.0 mass pct and [Al] = 0.0001 to 0.1 mass pct. The computed iso-oxygen content lines are also compared to the dissolved oxygen concentration estimated in the present study (Table II). The computed values are slightly larger than the values estimated from the slag-metal equilibria. Even though the exact reason for this discrepancy is not so clearly understood at this time, it is considered that there are some regions in the thermodynamic databases to be improved for the highly-alloyed melts such as stainless steel.[16]

The slope of the phase boundary between spinel (mainly $MgAl_2O_4$) and liquid oxide (Mg-Al-Ti-O) is nearly constant in the composition range of [Ti] > 0.01 mass pct and [Al] > 0.002 mass pct, whereas the spinel phase would not be formed at [Al] < 0.001 mass pct irrespective of titanium concentration. Moreover, it is of interest that some experimental points are relatively close to the spinel-liquid–phase boundary, indicating that the inclusions could be spinel + liquid oxide heterogeneous system. This will be systematically examined through the phase diagram study as follows.

The composition of the inclusions is plotted on the $MgO\text{-}Al_2O_3\text{-}TiO_x$ ternary phase diagram (Figure 4), which was computed by using FACTSAGE 5.5 program with the FACT53 and FToxid databases at 1873 K and $p_{O_2} = 10^{-13}$atm, which corresponds to the average value of oxygen activity (Figure 2) based on Eqs. [8] and [9].[20]

$$\frac{1}{2}O_2\ (g) = [O] \qquad [8]$$

$$\log\ K_{[8]} = \log\ \left[\frac{a_O}{p_{O_2}^{1/2}}\right] = \frac{6120}{T} + 0.18 \qquad [9]$$

In Figure 4, four solid phases such as spinel, Al_2O_3, MgO, and pseudobrookite (mainly Ti_3O_5) are in equilibrium with the liquid phase. The present phase diagram is relatively similar to those calculated by Kaufman and one of the authors (HRG) and co-workers.[8,35,36] However, because of the differences not only in the oxygen potential but also in thermodynamic models used in each study, there are some differences in the phase diagrams, especially in the area of fully liquid phase. It is noticeable that the inclusions in the steel melts equilibrated with the relatively basic slags ($B > 1.7$) are located in the spinel + liquid region, while those in equilibrium with the less basic ($B < 1.7$) slags are mostly in the liquid single phase. This is qualitatively in fair correspondence to the stability diagram discussed in Figure 3. Here, the basicity of the slags B is defined as given in Eq. [10].

$$B = \frac{(\text{mass pct CaO} + \text{mass pct MgO})}{(\text{mass pct SiO}_2 + \text{mass pct Al}_2\text{O}_3)} \qquad [10]$$

The representative morphology of the inclusions in each case (marked as (a) and (b) in Figure 4) is shown in Figure 5. However, in cases of relatively high concentration of titanium and aluminum (18M-9 and 18M-10 in Table II), the composition of the inclusions was found to be in the spinel + liquid region, although the less basic slags are equilibrated. The thermodynamic effect of the compositions of steel and slag on the inclusions will be discussed in detail in Section B.

In order to quantitatively investigate the composition of the inclusions, the ratio of tri- and tetravalent titanium in liquid phase has also been calculated by the FACTSAGE 5.5 program and is shown in Figure 6 as a function of the (mass pct MgO)/(mass pct Al_2O_3) ratio. The ratio of (mass pct Ti^{3+}) to (mass pct Ti^{3+} + mass pct Ti^{4+}) slightly increases by increasing the (mass pct MgO)/(mass pct Al_2O_3) ratio, regardless of

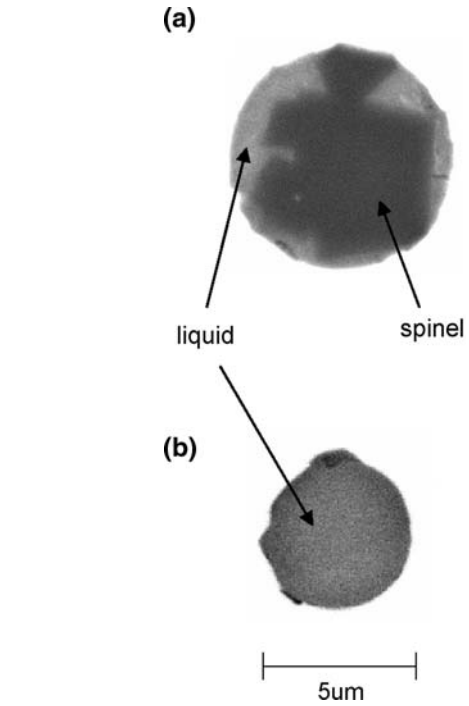

Fig. 5—Representative morphology of inclusions observed by SEM-EDS ((*a*) and (*b*) are marked in Fig. 4).

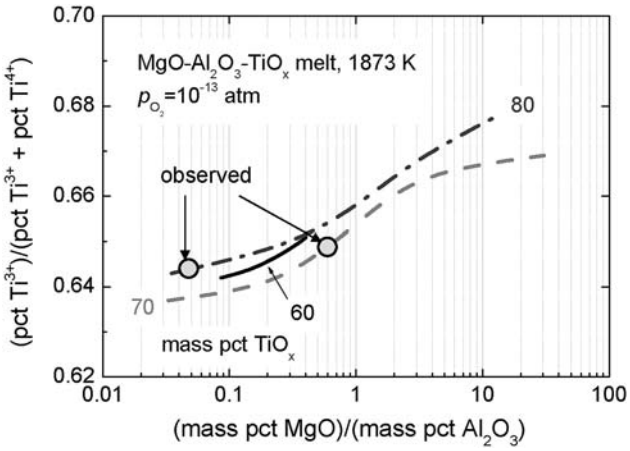

Fig. 6—Computed ratio of (mass pct Ti^{3+}) to (mass pct Ti^{3+} + mass pct Ti^{4+}) in liquid phase of the MgO-Al_2O_3-TiO_x inclusion system at 1873 K and $p_{O_2} = 10^{-13}$atm.

total content of titanium oxide. Nevertheless, it is considered from this calculation that the relative amount of Ti^{3+} would be more dominant than that of Ti^{4+} in the present MgO-Al_2O_3-TiO_x ternary system at 1873 K and $p_{O_2} = 10^{-13}$atm.

B. *Effect of Thermodynamic Function of Steel and Slag Components on the Composition of Inclusions in Fe-11Cr Steel Equilibrated with CaO-SiO_2-MgO-Al_2O_3-CaF_2 (-TiO_2) Slags*

The effect of alumina content in the slag on the concentration of alumina in the inclusions is shown in

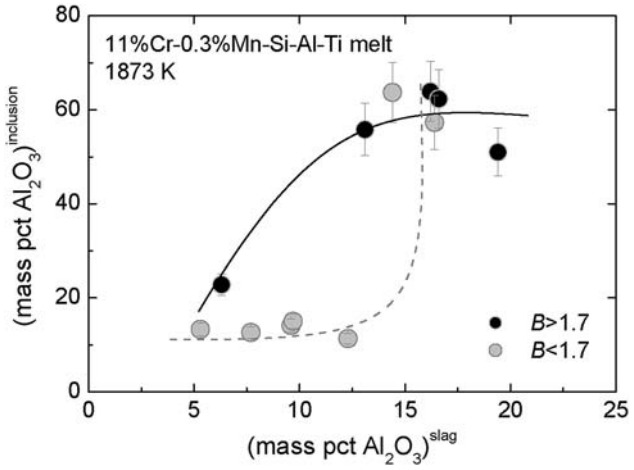

Fig. 7—Relationship of alumina content between inclusions and top slags at 1873 K.

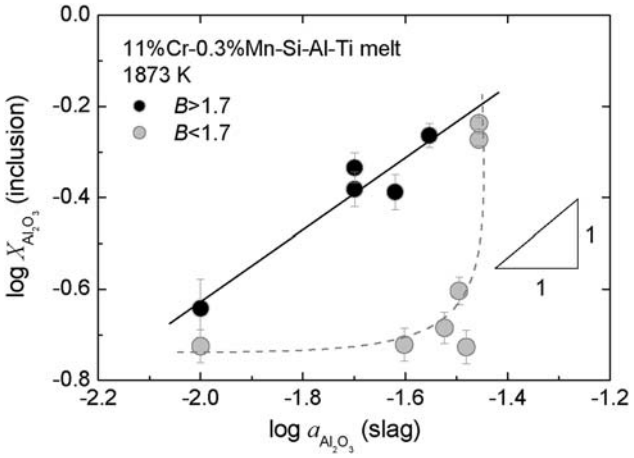

Fig. 8—Relationship between mole fraction of alumina in inclusions and activity of alumina in slags at 1873 K in logarithmic scale.

Figure 7 at 1873 K. The concentration of Al_2O_3 in the inclusions increases with increasing Al_2O_3 content in the relatively basic ($B > 1.7$) slags. However, there is no effect at Al_2O_3 content less than about 15 mass pct in the less basic ($B < 1.7$) slag, followed by an abrupt increase at about (Al_2O_3) = 15 mass pct. This tendency can be discussed more quantitatively by taking the activity-mole fraction relationship into account, as shown in Figure 8. The mole fraction of alumina in the inclusions log $X_{Al_2O_3}$ linearly increases with increasing activity of alumina log $a_{Al_2O_3}$ in the basic slags, with the slope of about 0.80 ($r^2 = 0.91$), which is close to unity. This indicates that the activity coefficient of alumina in the inclusions would probably be constant when the basic ($B > 1.7$) slags are in equilibrium with the steel melts, whereas the stability of alumina in the inclusions could significantly be affected by the reaction between less basic ($B < 1.7$) but high alumina potential ($a_{Al_2O_3} > 0.03$) slags and the steel melts.

As shown in Figure 4, the composition of the inclusions could be grouped into the spinel + liquid and

liquid oxides. Hence, the formation tendency of the spinel phase can qualitatively be estimated by considering the variation of the ratio of (MgO) × (Al_2O_3) to (Ti_2O_3) in the inclusions as the thermodynamic properties of the steel and slag phases change. The effect of the activities of magnesium, aluminum, titanium, and oxygen in molten steel on the mole ratio (MgO) × (Al_2O_3)/(Ti_2O_3) can be discussed based on the following equations.[18,26,37]

$$(\mathrm{MgO})^{\text{inclusion}} = [\mathrm{Mg}] + [\mathrm{O}],$$
$$\log K_{\mathrm{Mg}} = \log \left[\frac{a_{\mathrm{Mg}} \times a_{\mathrm{O}}}{a_{\mathrm{MgO}}}\right] = -\frac{4700}{T} - 4.28 \quad [11]$$

$$\log X_{\mathrm{MgO}} = \log a_{\mathrm{Mg}} + \log a_{\mathrm{O}} - \log \gamma_{\mathrm{MgO}} - \log K_{\mathrm{Mg}} \quad [12]$$

$$(\mathrm{Al_2O_3})^{\text{inclusion}} = 2[\mathrm{Al}] + 3[\mathrm{O}],$$
$$\log K_{\mathrm{Al}} = \log \left[\frac{a_{\mathrm{Al}}^2 \times a_{\mathrm{O}}^3}{a_{\mathrm{Al_2O_3}}}\right] = -\frac{45{,}300}{T} + 11.62 \quad [13]$$

$$\log X_{\mathrm{Al_2O_3}} = 2\log a_{\mathrm{Al}} + 3\log a_{\mathrm{O}} - \log \gamma_{\mathrm{Al_2O_3}} - \log K_{\mathrm{Al}} \quad [14]$$

$$(\mathrm{Ti_2O_3})^{\text{inclusion}} = 2[\mathrm{Ti}] + 3[\mathrm{O}],$$
$$\log K_{\mathrm{Ti}} = \log \left[\frac{a_{\mathrm{Ti}}^2 \times a_{\mathrm{O}}^3}{a_{\mathrm{Ti_2O_3}}}\right] = -\frac{44{,}240}{T} + 13.0 \quad [15]$$

$$\log X_{\mathrm{Ti_2O_3}} = 2\log a_{\mathrm{Ti}} + 3\log a_{\mathrm{O}} - \log \gamma_{\mathrm{Ti_2O_3}} - \log K_{\mathrm{Ti}} \quad [16]$$

By combining Eqs. [12], [14], and [16], the following equation can be deduced.

$$\log \left(\frac{X_{\mathrm{MgO}} \times X_{\mathrm{Al_2O_3}}}{X_{\mathrm{Ti_2O_3}}}\right) = \log \left[\frac{a_{\mathrm{Mg}} \times a_{\mathrm{Al}}^2 \times a_{\mathrm{O}}}{a_{\mathrm{Ti}}^2}\right] + \log \left(\frac{\gamma_{\mathrm{Ti_2O_3}}}{\gamma_{\mathrm{MgO}} \times \gamma_{\mathrm{Al_2O_3}}}\right) + \text{constant} \quad [17]$$

In Eq. [17], assuming that the second term of the activity coefficient ratio on the right side would be constant, on a logarithmic scale the mole ratio of the inclusion components on the left side is in direct proportion to the activity ratio of Mg, Al, O, and Ti in molten steel. In order to calculate the activity of each alloy component, the activity coefficient of each element in molten steel was calculated based on Eq. [7] and the interaction parameters listed in Table III.[12,18,20–29] In Figure 9, the log $\left(X_{\mathrm{MgO}} \times X_{\mathrm{Al_2O_3}}/X_{\mathrm{Ti_2O_3}}\right)$ of the inclusions is plotted against the log $\left[a_{\mathrm{Mg}} \times a_{\mathrm{Al}}^2 \times a_{\mathrm{O}}/a_{\mathrm{Ti}}^2\right]$ of the steel melts. A linear relationship between them can be found with a slope of 1.1 (r^2 = 0.8), which is very close to unity expected in Eq. [17] within the composition range investigated in the present study. This means that the inclusion-steel system would be in equilibrium and that the formation tendency of the spinel-type inclusions can be predicted from the thermodynamics of deoxidizing elements and oxygen in ferritic stainless steel melts.

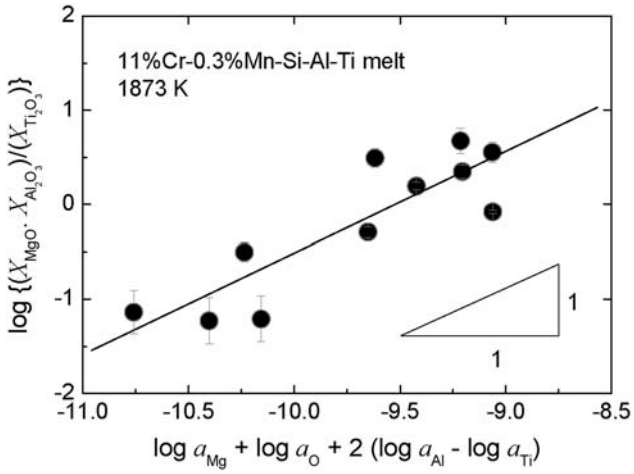

Fig. 9—Effect of activities of Mg, Al, Ti, and O, log $\left[a_{\mathrm{Mg}} \times a_{\mathrm{Al}}^2 \times a_{\mathrm{O}}/a_{\mathrm{Ti}}^2\right]$ on composition of inclusions, log $\left(X_{\mathrm{MgO}} \times X_{\mathrm{Al_2O_3}}/X_{\mathrm{Ti_2O_3}}\right)$ in steel melts at 1873 K.

On the other hand, the spinel-type inclusions have been proposed to appear when the highly basic slags are equilibrated with the steel melts based on the following reactions, for example:[14,16,17,38–41]

$$2(\mathrm{MgO})^{\text{slag or refractory}} + [\mathrm{Si}] = (\mathrm{SiO_2})^{\text{slag or inclusion}} + 2[\mathrm{Mg}] \quad [18]$$

$$\log K_{[18]} = \log \left[\frac{a_{\mathrm{SiO_2}} \times a_{\mathrm{Mg}}^2}{a_{\mathrm{MgO}}^2 \times a_{\mathrm{Si}}}\right] = \frac{15{,}200}{T} - 16.96 \quad [19]$$

$$[\mathrm{Mg}] + [\mathrm{O}] = (\mathrm{MgO})^{\text{inclusion}} \quad [20]$$

$$\log K_{[20]} = \log \left[\frac{a_{\mathrm{MgO}}}{a_{\mathrm{Mg}} \times a_{\mathrm{O}}}\right] = \frac{4700}{T} + 4.28 \quad [21]$$

Therefore, assuming that the activity of O^{2-} ions would be proportional to that of CaO, it is very meaningful to investigate the effect of the activity of CaO in the slag on the formation behavior of spinel-type inclusions in molten steel. In Figure 10, the log $\left(X_{\mathrm{MgO}} \times X_{\mathrm{Al_2O_3}}/X_{\mathrm{Ti_2O_3}}\right)$ of the inclusions is shown as a function of the activity of CaO, log a_{CaO} in the slag at 1873 K,

which was calculated by using FACTSAGE 5.5 program. It is hard to find the organic relationship between them. This phenomenon could be explained by the thermodynamic relationship between slag components. Actually, because the MgO crucible was used in the steel-slag equilibrium experiments in this study, the slag was saturated by MgO, and thus, the activity of MgO could be taken into unity through the present compositions. The activity of TiO_2 in the slag would decrease with increasing activity of CaO due to the relatively acidic characteristics of TiO_2 in the calcium silicate melts.[42] This tendency is also in good accordance with the calculated result by FACTSAGE 5.5 program in this study. However, the alumina probably behaves as a basic oxide in the relatively low a_{CaO} region, whereas it behaves as an acidic oxide in the relatively high a_{CaO} region in the calcium aluminosilicate melts.[43,44] Consequently, because of the changes in the chemical potential of slag components, the value of $\log\left(X_{MgO} \times X_{Al_2O_3}/X_{Ti_2O_3}\right)$ would exhibit a hump, as shown in Figure 10.

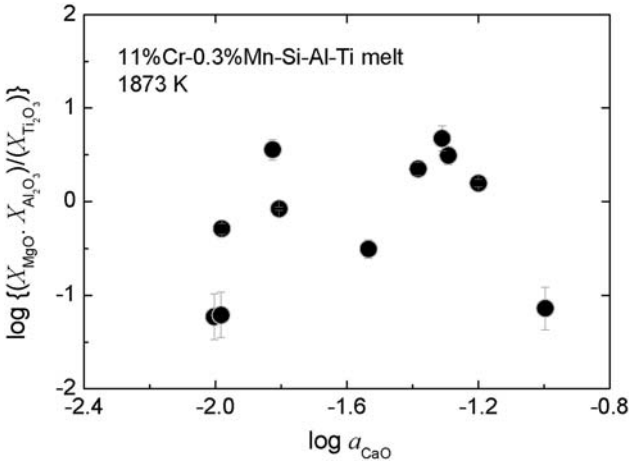

Fig. 10—Effect of activity of lime $\log a_{CaO}$ in slag on composition of inclusions, $\log\left(X_{MgO} \times X_{Al_2O_3}/X_{Ti_2O_3}\right)$ in steel melts at 1873 K.

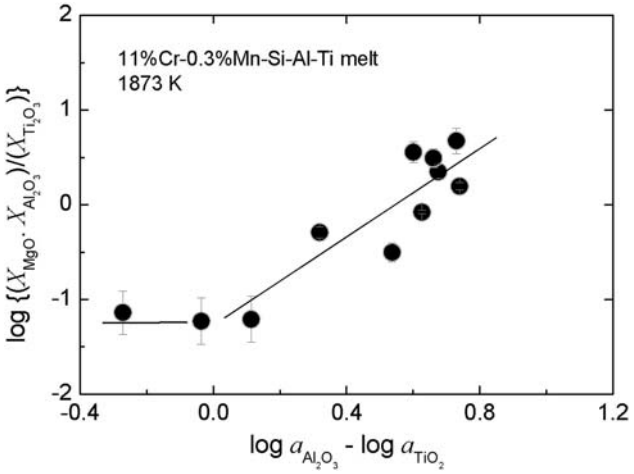

Fig. 11—Effect of activity ratio of Al_2O_3 to TiO_2 $\log\left(a_{Al_2O_3}/a_{TiO_2}\right)$ in slag on composition of inclusions, $\log\left(X_{MgO} \times X_{Al_2O_3}/X_{Ti_2O_3}\right)$ in steel melts at 1873 K.

Finally, the relationship between the $\log\left(X_{MgO} \times X_{Al_2O_3}/X_{Ti_2O_3}\right)$ of the inclusions and the $\log\left(a_{Al_2O_3}/a_{Ti_2O_3}\right)$ of the top slag at 1873 K is shown in Figure 11. The activity of TiO_2 was calculated by using the FACTSAGE 5.5 program. It is of interest that the value of $\log\left(X_{MgO} \times X_{Al_2O_3}/X_{Ti_2O_3}\right)$ is very low and nearly constant when the activity of Al_2O_3 is less than that of TiO_2 in the slag, followed by linear increase with increasing $\log\left(a_{Al_2O_3}/a_{Ti_2O_3}\right)$. As discussed in Figure 10, the activity of MgO in the slag could be fixed in the present study. Hence, the thermodynamic driving force for the formation of spinel-type inclusions is very low in the composition of $\left(a_{Al_2O_3}/a_{Ti_2O_3}\right) < 1$, while it linearly increases by increasing the activity ratio of Al_2O_3 to TiO_2 in the slag at $\left(a_{Al_2O_3}/a_{Ti_2O_3}\right) > 1$. This means that the activity of Al_2O_3 and TiO_2 in the slag significantly affects the formation behavior of the spinel-type inclusions in Ti-stabilized ferritic stainless steel melts, especially in the case of MgO saturated slag and magnesia or dolomite refractory lining materials are used.

IV. CONCLUSIONS

The equilibration between $CaO\text{-}SiO_2\text{-}MgO\text{-}Al_2O_3\text{-}CaF_2$ (-TiO_2) slag and Fe-11 mass pct Cr ferritic stainless steel melts was investigated at 1873 K in order to clarify the effect of aluminum and titanium addition, as well as that of slag composition, on the formation of complex oxide inclusions. The following conclusions could be drawn.

1. The activity of oxygen calculated from the classical Wagner formalism changes from about $a_O = 0.0002$ to 0.001, and the values of a_O from [Al]/(Al_2O_3) and that from [Si]/(SiO_2) equilibria are in relatively good correspondence to each other with some scatters.
2. The phase stability diagram of the inclusions and the equilibrium iso-[O] lines in the Fe-11 mass pct Cr-0.5 mass pct Si-0.3 mass pct Mn-0.0005 mass pct Mg stainless steel melts was constructed by using FACTSAGE 5.5 program as a function of Al and Ti contents. However, the computed iso-[O] lines were relatively larger than the values estimated from the slag-metal equilibria.
3. The composition of the inclusions could be plotted on the computed $MgO\text{-}Al_2O_3\text{-}TiO_x$ phase diagram. The inclusions in the steel melts equilibrated with the basic slags are located in the spinel + liquid region, while those in equilibrium with the less basic slags are mostly in the liquid single phase. This is in good accordance to the observed morphology of the inclusions. However, in cases of high concentration of Ti and Al, the inclusions were found to be spinel + liquid, although the less basic slags are equilibrated.
4. The $\log\left(X_{MgO} \times X_{Al_2O_3}/X_{Ti_2O_3}\right)$ of the inclusions was expressed as a linear function of the $\log\left[a_{Mg} \times a_{Al}^2 \times a_O/a_{Ti}^2\right]$ of the steel melts with a slope of unity theoretically expected.

5. The $\log\left(X_{MgO} \times X_{Al_2O_3}/X_{Ti_2O_3}\right)$ is very low and nearly constant when the activity of Al_2O_3 is less than that of TiO_2 in the slag saturated by MgO, whereas it linearly increases by increasing the $\log\left(a_{Al_2O_3}/a_{Ti_2O_3}\right)$ at $\left(a_{Al_2O_3}/a_{Ti_2O_3}\right) > 1$.

REFERENCES

1. M. Hasegawa, S. Maruhashi, Y. Kamidate, Y. Muranaka, and F. Hoshi: *Tetsu-to-Hagané*, 1984, vol. 70, pp. 1704–11.
2. Y. Gao and K. Sorimachi: *ISIJ Int*., 1993, vol. 33, pp. 291–97.
3. R. Maddalena, R. Rastogi, S. Bassem, and A.W. Cramb: *Iron Steelmaker*, 2000, vol. 27, pp. 71–79.
4. R.C. Nunnington and N. Sutcliffe: *59th Electric Furnace Conf. Proc*., Phoenix, AZ, Nov. 11–14, 2001, ISS, Warrendale, PA, 2002, pp. 361–94.
5. H. Zheng, W. Chen, and Y. Hu: *AISTech 2004: Iron & Steel Tech. Conf. Proc*., Nashville, TN, Sept. 15–17, 2004, AIST, Warrendale, PA, 2004, pp. 937–45.
6. J.W. Kim, S.K. Kim, D.S. Kim, Y.D. Lee, and P.K. Yang: *ISIJ Int*., 1996, vol. 36, pp. S140–S143.
7. D.S. Kim, J.H. Park, Jong H. Park, S.B. Lee, and H.G. Lee: *Rev. Metall*., 2004, vol. 4, pp. 291–99.
8. H. Fujimura, S. Tsuge, Y. Komizo, and T. Nishizawa: *Tetsu-to-Hagané*, 2001, vol. 87, pp. 707–12.
9. T. Koseki and H. Inoue: *J. Jpn. Inst. Met*., 2001, vol. 65, pp. 644–51.
10. B. Granier, R. Renard, and J.P. Coultures: *High Temp. Ceramics (France)*, 1980, vol. 17, pp. 235–47.
11. L. Liao and R.J. Fruehan: *Iron Steelmaker*, 1989, vol. 16, pp. 91–97.
12. S.K. Jo, B. Song, and S.H. Kim: *Metall. Mater. Trans. B*, 2002, vol. 33B, pp. 703–09.
13. J.H. Park and D.S. Kim: *Metall. Mater. Trans. B*, 2005, vol. 36B, pp. 495–502.
14. G. Okuyama, K. Yamaguchi, S. Takeuchi, and K. Sorimachi: *ISIJ Int*., 2000, vol. 40, pp. 121–28.
15. J.H. Park and D.J. Min: *Mater. Trans*., 2006, vol. 47, pp. 2038–43.
16. J.H. Park and Y.B. Kang: *Metall. Mater. Trans. B*, 2006, vol. 37B, pp. 791–98.
17. J.H. Park: *Mater. Sci. Eng. A*, 2008, vol. 472, pp. 43–51.
18. H. Itoh, M. Hino, and S. Ban-ya: *Tetsu-to-Hagané*, 1997, vol. 83, pp. 773–78.
19. K. Suzuki, S. Ban-ya, and M. Hino: *ISIJ Int*., 2001, vol. 41, pp. 813–17.
20. *Steelmaking Data Sourcebook, The Japan Society for the Promotion of Science*, 19th Committee of Steelmaking, Gordon and Breach Science Publications, New York, NY, 1988, pp. 273–325.
21. H.R. Gaye: in *The Making, Shaping and Treating of Steel*, 11th ed., Casting Volume, The AISE Steel Foundation, Pittsburgh, PA, 2003, pp. 1–8.
22. Z. Hong, X. Wu, and C. Kun: *Steel Res*., 1995, vol. 66, pp. 72–76.
23. K. Morita, M. Ohta, A. Yamada, and M. Ito: *ICS 2005 Conf. Proc*., Charlotte, NC, May 9–12, 2005, AIST, Warrendale, PA, 2005, pp. 15–22.
24. J.J. Pak, Y.S. Jeong, I.K. Hong, W.Y. Cha, D.S. Kim, and Y.Y. Lee: *ISIJ Int*., 2005, vol. 45, pp. 1106–11.
25. J.J. Pak, J.T. Yoo, Y.S. Jeong, S.J. Tae, S.M. Seo, D.S. Kim, and Y.D. Lee: *ISIJ Int*., 2005, vol. 45, pp. 23–29.
26. J.J. Pak, J.J. Jo, S.I. Kim, W.I. Kim, T.I. Chung, S.M. Seo, J.H. Park, and D.S. Kim: *ISIJ Int*., 2007, vol. 47, pp. 16–24.
27. J.D. Seo and S.H. Kim: *Steel Res*., 2000, vol. 71, pp. 101–06.
28. T. Itoh, T. Nagasaka, and M. Hino: *ISIJ Int*., 2000, vol. 40, pp. 1051–58.
29. K. Takahashi and M. Hino: *High Temp. Mater. Proc*., 2000, vol. 19, pp. 1–10.
30. H. Ohta and H. Suito: *Metall. Mater. Trans. B*, 1998, vol. 29B, pp. 119–29.
31. J. Lehmann and H. Gaye: *82nd ISS Steelmaking Conf. Proc*., Chicago, IL, Mar. 21–24, 1999, ISS, Warrendale, PA, 1999, pp. 463–70.
32. H. Gaye, M. Faral, and J. Lehmann: *Rev. Metall*., 2003, vol. 2, pp. 125–34.
33. http://www.factsage.com/.
34. I.H. Jung, S.A. Devterov, and A.D. Pelton: *ISIJ Int*., 2004, vol. 44, pp. 527–36.
35. L. Kaufman: *Physica B and C*, 1988, vol. 150, pp. 99–114.
36. F. Ruby-Meyer, J. Lehmann, and H. Gaye: *Scand. J. Metall*., 2000, vol. 29, pp. 206–12.
37. H. Itoh, M. Hino, and S. Ban-ya: *Tetsu-to-Hagané*, 1997, vol. 83, pp. 623–28.
38. T. Nishi and K. Shinme: *Tetsu-to-Hagané*, 1998, vol. 84, pp. 97–102.
39. T. Nishi and K. Shinme: *Tetsu-to-Hagané*, 1998, vol. 84, pp. 837–43.
40. J.H. Park: *Calphad*, 2007, vol. 31, pp. 428–37.
41. J.H. Park: *Metall. Mater. Trans. B*, 2007, vol. 38B, pp. 657–63.
42. C.O. Ariyo and L.E.K. Holappa: *Scand. J. Metall*., 2002, vol. 31, pp. 385–92.
43. P. Kozakevitch: *Rev. Metall*., 1960, vol. 57, pp. 149–60.
44. J.H. Park, D.J. Min, and H.S. Song: *Metall. Mater. Trans. B*, 2004, vol. 35B, pp. 269–75.
45. C.H.P. Lupis: *Chemical Thermodynamics of Materials*, Prentice Hall, New York, NY, pp. 255–57.